Iranian Journal of Science & Technology, Transaction B: Engineering, Vol. 34, No. B2, pp 149-165
Printed in The Islamic Republic of Iran, 2010

A COMPLETE TREATMENT OF THERMO-MECHANICAL ALE ANALYSIS; PART 2: FINITE ELEMENT EQUATIONS AND APPLICATIONS*

Y. TADI BENI, M.R. MOVAHHEDY** AND G.H. FARRAHI

School of Mechanical Engineering, Sharif University of Technology, Tehran, I. R. of Iran
Email: movahhed@sharif.edu

Abstract– In the first part of this paper series, a complete formulation for fully coupled ALE analysis of large deformation solid mechanic problems was developed. The formulation incorporated inertial, rate and thermal effects, and the treatment of rate and temperature dependent constitutive equations were presented. In this part, the ALE equations are discretized to form finite element equations. An algorithm for the treatment of mesh motion is described and example problems are presented to demonstrate the capability of the proposed formulation.

Keywords– Arbitrary Lagrangian Eulerian, finite element method, large deformation, implicit dynamic analysis, thermo-mechanical, viscoplastic

1. FINITE ELEMENT EQUATIONS

In the first part of this paper, the ALE forms of equations of motion and energy balance were presented. In this part, we discretize these equations to put it in finite element form.

a) Discretization of equation of motion

The ALE finite element equations are obtained from discretization of Eqs. (29) in the first part for Jaumann rate. The final form of ALE finite element equation of motion may be cast in the standard form

$$\begin{aligned} &{}^t\mathbf{M}^L\,{}^{t+\Delta t}\ddot{\mathbf{u}}^{(i)} + {}^t\mathbf{N}^1\,{}^{t+\Delta t}\dot{\mathbf{u}}^{(i)} + {}^t\mathbf{K}^m\mathbf{u}^{(i)} - {}^t\mathbf{K}^g\mathbf{u}^{g(i)} = {}^{t+\Delta t}\mathbf{f}^{ext} - {}^t\boldsymbol{f}^T - {}^{t+\Delta t}\mathbf{f}^{(i-1)} - {}^t\mathbf{M}^A\,{}^{t+\Delta t}\ddot{\mathbf{u}}^{(i-1)} \\ &-({}^t\mathbf{N}^2 - {}^t\mathbf{N}^3 + {}^t\mathbf{N}^4)\,{}^{t+\Delta t}\dot{\mathbf{u}}^{(i-1)} \end{aligned} \tag{1}$$

In the above equation, ${}^t\mathbf{M}^L$ is the Lagrangian mass matrix given by

$${}^t\mathbf{M}^L = \int_{{}^tV} {}^t\rho(\mathbf{H})^T\mathbf{H}\,{}^tdV \tag{2}$$

${}^t\mathbf{K}^m$ is the stiffness matrix related to material deformation, ${}^t\mathbf{K}^g$ is the stiffness term arising from grid motion and ${}^{t+\Delta t}\mathbf{f}^{ext}$ is the vector of externally applied load. Using the Jaumann rate of stress, ${}^t\mathbf{K}^m$ can be expanded into three parts as given below;

$${}^t\mathbf{K}^m = {}^t\mathbf{K}^L + {}^t\mathbf{K}^1 + {}^t\mathbf{K}^2 \tag{3}$$

where ${}^t\mathbf{K}^L$ is the Lagrangian stiffness matrix and ${}^t\mathbf{K}^1$, ${}^t\mathbf{K}^2$ are geometric stiffness matrices defined as

$${}^t\mathbf{K}^L = \int_{{}^tV} ({}_t\mathbf{B}^L)^T\,{}^t\mathbf{C}^{EP}\,{}_t\mathbf{B}^L\,{}^tdV \tag{4}$$

*Received by the editors January 28, 2009; Accepted October 12, 2009.
**Corresponding author

$$ {}^{t}\mathbf{K}^{1} = \int_{{}^{t}V} ({}_{t}\mathbf{B}^{A1})^{T}\, {}^{t}\mathbf{S}^{A1}\, {}_{t}\mathbf{B}^{A1}\, {}^{t}dV - \int_{{}^{t}V} ({}_{t}\mathbf{B}^{A2})^{T} ({}^{t}\mathbf{S}^{A1})^{T}\, {}_{t}\mathbf{B}^{A2}\, {}^{t}dV + \int_{{}^{t}V} ({}_{t}\mathbf{B}^{A2})^{T} ({}^{t}\mathbf{S}^{A1})^{T}\, {}_{t}\mathbf{B}^{A1}\, {}^{t}dV \tag{5} $$

$$ {}^{t}\mathbf{K}^{2} = -\int_{{}^{t}V} ({}_{t}\mathbf{B}^{A1})^{T}\, {}^{t}\mathbf{S}^{A1}\, {}_{t}\mathbf{B}^{A2}\, {}^{t}dV + \int_{{}^{t}V} ({}_{t}\mathbf{B}^{A1})^{T}\, {}^{t}\mathbf{S}^{A3}\, {}_{t}\mathbf{B}^{A2}\, {}^{t}dV + \int_{{}^{t}V} ({}_{t}\mathbf{B}^{A3})^{T}\, {}^{t}\mathbf{S}^{A2}\mathbf{H}\, {}^{t}dV \tag{6} $$

In the Eq. (4) ${}^{t}\mathbf{C}^{EP}$ is the elastic-plastic material constitutive matrix. For a viscoplastic material, this matrix may be substituted by the defined equation of part 1. Similarly, the stiffness matrix due to grid motion is defined as

$$ {}^{t}\mathbf{K}^{g} = \int_{{}^{t}V} ({}_{t}\mathbf{B}^{A3})^{T}\, {}^{t}\mathbf{S}^{A2}\mathbf{H}\, {}^{t}dV + 2\int_{{}^{t}V} ({}_{t}\mathbf{B}^{A2})^{T} ({}^{t}\mathbf{S}^{A1})^{T}\, {}_{t}\mathbf{B}^{A1}\, {}^{t}dV \tag{7} $$

and the internal force vector is given as

$$ {}^{t+\Delta t}\mathbf{f}^{(i-1)} = \int_{{}^{t+\Delta t}V} ({}_{t+\Delta t}\mathbf{B}^{L(i-1)})^{T}\, {}^{t+\Delta t}\boldsymbol{\sigma}^{(i-1)}\, {}^{t+\Delta t}dV \tag{8} $$

The parameter ${}^{t}\boldsymbol{f}^{T}$ in the above equation is the thermal loading vector given by

$$ {}^{t}\boldsymbol{f}^{T} = \int_{{}^{t}V} \left({}_{t}\mathbf{B}^{L}\right)^{T}\, {}_{t}\boldsymbol{\eta}\, \dot{T}\, {}^{t}dV \tag{9} $$

The definitions of matrices ${}_{t}\mathbf{B}^{L}$, ${}_{t}\mathbf{B}^{A1}$, ${}_{t}\mathbf{B}^{A2}$, ${}_{t}\mathbf{B}^{A3}$, ${}^{t}\mathbf{S}^{A1}$, ${}^{t}\mathbf{S}^{A2}$, ${}^{t}\mathbf{S}^{A3}$, $\mathbf{H}$, ${}^{t}\mathbf{N}^{1}$, ${}^{t}\mathbf{N}^{2}$, ${}^{t}\mathbf{N}^{3}$, ${}^{t}\mathbf{N}^{4}$, ${}_{t}\boldsymbol{\eta}$ and ${}^{t}\mathbf{M}^{A}$ are given in the appendix. Note that matrix ${}_{t}\mathbf{B}^{A3}$ above includes terms involving second derivatives of shape functions, thus C1-continuity is required of elements used to guarantee convergence. For treatment of the dynamic term, the Newmark implicit integration scheme is used as given below

$$ {}^{t+\Delta t}\mathbf{u}^{(i)} = {}^{t}\mathbf{u} + \Delta t\, {}^{t}\dot{\mathbf{u}} + (\Delta t)^{2}(\frac{1}{2} - \beta)\, {}^{t}\ddot{\mathbf{u}} + (\Delta t)^{2}\beta\, {}^{t+\Delta t}\ddot{\mathbf{u}}^{(i)} \tag{10} $$

$$ {}^{t+\Delta t}\dot{\mathbf{u}}^{(i)} = {}^{t}\dot{\mathbf{u}} + \Delta t(1-\gamma)\, {}^{t}\ddot{\mathbf{u}} + \Delta t\gamma\, {}^{t+\Delta t}\ddot{\mathbf{u}}^{(i)} \tag{11} $$

$$ {}^{t+\Delta t}\mathbf{u}^{(i)} = {}^{t+\Delta t}\mathbf{u}^{(i-1)} + \mathbf{u}^{i} \tag{12} $$

where β and γ are parameters controlling integration accuracy and stability. By substituting Eqs. (10), (11) and (12) into (1), the final ALE finite element equation can be written as

$$ \begin{aligned} &[\frac{1}{(\Delta t)^{2}\beta}\, {}^{t}\mathbf{M}^{L} + \frac{\gamma}{\Delta t\beta}\, {}^{t}\mathbf{N}^{1} + {}^{t}\mathbf{K}^{m}]\mathbf{u}^{(i)} - {}^{t}\mathbf{K}^{g}\mathbf{u}^{g(i)} = {}^{t+\Delta t}\mathbf{f}^{ext} - {}^{t+\Delta t}\mathbf{f}^{(i-1)} - {}^{t}\boldsymbol{f}^{T} \\ &-({}^{t}\mathbf{M}^{L} + {}^{t}\mathbf{M}^{A})\, {}^{t+\Delta t}\ddot{\mathbf{u}}^{(i-1)} - ({}^{t}\mathbf{N}^{1} + {}^{t}\mathbf{N}^{2} - {}^{t}\mathbf{N}^{3} + {}^{t}\mathbf{N}^{4})\, {}^{t+\Delta t}\dot{\mathbf{u}}^{(i-1)} \end{aligned} \tag{13} $$

b) Discretization of equation of energy

To discretize the equation of energy balance (Eq. (33) of part 1), a temporal incrementation of temperature is used based on backward difference approximation;

$$ {}^{t+\Delta t}\mathbf{T}^{(i)} = {}^{t+\Delta t}\mathbf{T}^{(i-1)} + \Delta t\, {}^{t+\Delta t}\mathbf{T}' \tag{14} $$

$$ {}^{t+\Delta t}\mathbf{T}^{(i)} = {}^{t+\Delta t}\mathbf{T}^{(i-1)} + \mathbf{T}^{(i)} \tag{15} $$

where i is the index of the increment. By discretization of Eq. (33) in part 1 and applying Eqs. (14) and (15), the final form of ALE finite element of balance of energy is given by

$$ {}^{t+\Delta t}\mathbf{K}^{(i-1)}\boldsymbol{T}^{(i)} = {}^{t+\Delta t}\mathbf{Q}_{\text{ext}} + {}^{t+\Delta t}\mathbf{Q}_{\text{c}}^{(\text{i-1})} - {}^{t+\Delta t}\mathbf{Q}_{\text{int}}^{(\text{i-1})} \tag{16} $$

where

$$ {}^{t+\Delta t}\mathbf{K}^{(i-1)} = {}^{t+\Delta t}\mathbf{C}_{\text{A}}^{(\text{i-1})} + \int_{t+\Delta t V} {}^{t+\Delta t}\left(\rho c_p\right)\mathbf{H}^T\mathbf{H}\,{}^{t+\Delta t}dv + \int_{t+\Delta t V} {}^{t+\Delta t}k^{(i-1)}\,{}_{\text{t}}\mathbf{B}^{\text{T}}\,{}_{\text{t}}\mathbf{B}\,{}^{t+\Delta t}dv + \int_{t+\Delta t S^c} {}^{t+\Delta t}h^{(i-1)}\mathbf{H}_{\text{s}}^{\text{T}}\mathbf{H}_{\text{s}}\,{}^{t+\Delta t}dS \tag{17} $$

$$ {}^{t+\Delta t}\mathbf{Q}_{\text{ext}} = \int_{t+\Delta t V} {}^{t+\Delta t}\left(\dot{W}\right)^{irr}\mathbf{H}^{\text{T}}\,{}^{t+\Delta t}dv \tag{18} $$

$$ {}^{t+\Delta t}\mathbf{Q}_{\text{c}}^{(\text{i-1})} = \int_{t+\Delta t S^c} {}^{t+\Delta t}h^{(i-1)}\mathbf{H}_{\text{s}}^{\text{T}}\left[\mathbf{H}_{\text{s}}\left({}^{t+\Delta t}T_{\infty} - {}^{t+\Delta t}T^{(i-1)}\right)\right]{}^{t+\Delta t}dS \tag{19} $$

$$ {}^{t+\Delta t}\mathbf{Q}_{\text{int}}^{(\text{i-1})} = {}^{t+\Delta t}\mathbf{Q}_{\text{A1}}^{(\text{i-1})} - {}^{t+\Delta t}\mathbf{Q}_{\text{A2}}^{(\text{i-1})} + \int_{t+\Delta t V} {}^{t+\Delta t}k^{(i-1)}\,{}_{\text{t}}\mathbf{B}^{\text{T}}\,{}_{\text{t}}\mathbf{B}\,{}^{t+\Delta t}\mathbf{T}^{\mathbf{(i-1)}}\,{}^{t+\Delta t}dV + \int_{t+\Delta t S^c} {}^{t+\Delta t}h^{(i-1)}\mathbf{H}_{\text{s}}^{\text{T}}\mathbf{H}_{\text{s}}\,{}^{t+\Delta t}\mathbf{T}^{\mathbf{(i-1)}}\,{}^{t+\Delta t}dS \tag{20} $$

The definitions of matrices ${}^{t+\Delta t}\mathbf{C}_{\text{A}}^{(\text{i-1})}$ and vectors ${}^{t+\Delta t}\mathbf{Q}_{\text{A1}}^{(\text{i-1})}$, ${}^{t+\Delta t}\mathbf{Q}_{\text{A2}}^{(\text{i-1})}$ and $\mathbf{H}$ are provided in the Appendix. The matrix ${}^{t+\Delta t}\mathbf{C}_{\text{A}}^{(\text{i-1})}$ and vector ${}^{t+\Delta t}\mathbf{Q}_{\text{A}}^{(\text{i-1})}$ are the convective terms arisen from ALE motion. Vector $\mathbf{H}_{\text{s}}$ is the vector of shape functions on the surface [1].

2. MESH MOTION

In the ALE method, the finite element mesh can be moved arbitrarily to maintain a homogenous mesh and to properly represent the boundary condition throughout the deformation process. Following reference [2], we use a simple mesh motion scheme which expresses the relationship between material and grid nodal displacement as

$$ \mathbf{u}^{g(i)} = \mathbf{a} + \mathbf{B}\,\mathbf{u}^{(i)} \tag{21} $$

where $\mathbf{a}$ and $\mathbf{B}$ coefficients are a vector and a matrix of appropriate parameters, respectively. This modified form of mesh motion equation allows a coupling between the degrees of freedom of a node, and is instrumental in specification of mesh sliding on external boundaries. Following [2], we use the transfinite-mapping method [3] for specifying mesh displacements within given boundaries. The finite element equilibrium Eq. (13) can be written in general form

$$ {}^{t}\mathbf{K}\,\mathbf{u}^{(i)} - {}^{t}\mathbf{K}^{g}\,\mathbf{u}^{g(i)} = \mathbf{f}^{(i)} - {}^{t}\boldsymbol{f}^{T} \tag{22} $$

where ${}^{t}\mathbf{K}$ and ${}^{t}\mathbf{K}^{g}$ are equivalent stiffness matrices and $\mathbf{f}^{(i)}$ is the incremental load vector. Equation (22) involves two sets of displacement variables; material displacements and grid displacements. In order to reduce the size of the solution vector, grid displacements may be eliminated by expressing them in terms of material displacements. This is achieved by substituting Eq. (21) into Eq. (22). This substitution is performed at the element level, and thus, grid displacement is condensed out of the global equation of motion

$$ \left({}^{t}\mathbf{K} - {}^{t}\mathbf{K}^{g}\mathbf{B}\right)\mathbf{u}^{(i)} = \mathbf{f}^{(i)} + {}^{t}\mathbf{K}^{g}\mathbf{a} - {}^{t}\boldsymbol{f}^{T} \tag{23} $$

The conventional finite element assembly and elimination techniques may now be applied directly to solve material displacements.

3. SOLUTION PROCEDURE

The equations describing material deformation and thermal flow form a set of governing equations that must be solved simultaneously at each incremental step of the nonlinear analysis. These sets of equations can be solved either in coupled form (Direct method), or in staggered form (Sequential method). The coupled approach is more realistic, but is computationally very intensive because it involves handling a large system of equations at every increment. This type of approach is necessary only if a large variation of temperature occurs within an increment. However, when the increments are small and temperature is gradually generated and spread over the analysis region, a staggered approach is preferred because it splits the coupled problem within an increment into a deformation analysis for a known temperature field followed by thermal analysis for a known deformation field, and iterating between the two stages until convergence. In this work, we use the staggered schemes to handle the ALE thermomechanical problem. In the staggered ALE analysis, the material and grid velocities calculated at each incremental step in the deformation part are used to solve the temperature field in the heat transfer analysis that follows it. At the end of the incremental step, the temperature field is transferred to the ALE mesh in the same way the other variables are mapped. It must be emphasized that the sequential treatment of the mechanical and thermal parts does not affect the true nature of fully coupled ALE formulation, because the material and grid deformation still occur simultaneously as required by a coupled formulation and the material and grid motions exist in both parts of the solution.

4. APPLICATIONS

In this section, example problems are presented to demonstrate the capability of the developed thermo-mechanical formulation in the simulation of some of the benchmark problems of solid mechanics.

a) One dimensional elastic-plastic wave propagation problem

A benchmark problem for verification of dynamic ALE formulations presented in the literature is the one dimensional wave propagation in an infinitely long elastic-plastic rod. This problem has been previously reported in references [4], [5], [6] and [7], and is solved here to demonstrate the dynamic capability of the presented formulation. The schematic statement of the problem and the loading function are shown in Fig. 1.

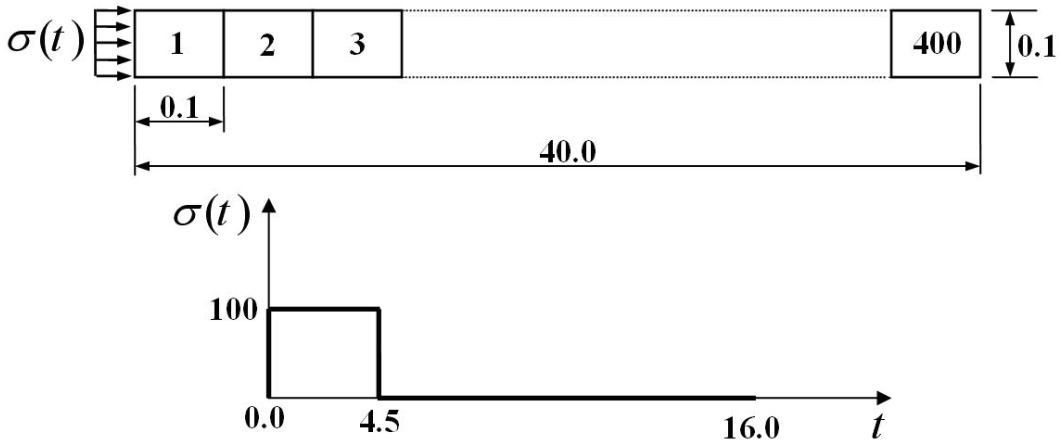

Fig. 1. Schematic statement of the one dimensional wave propagation problem

The infinitely long rod with elastic-plastic, linear hardening material behavior is discretized into 400 plane stress square elements of size 0.1. The material properties are: Young's modulus =10000.0, density=10000.0, plastic modulus=3333.33, Yield stress=75.0 and Poisson's ratio =0.0. A square compressive stress wave with an amplitude of 100.0 and width of 4.5. is applied to the left-hand side of the rod. Figure 1 shows the profile of the stress wave.

Figures 2 and 3 show the propagation of longitudinal stress wave in the rod at time t=16sec, in comparison with the expected analytical solution for elastic and elastic-plastic cases, respectively.

It is observed that the ALE results are generally in good agreement with the analytical solution and the oscillations observed in the present solution are less than the oscillations reported in some of the other solutions reported in the literature.

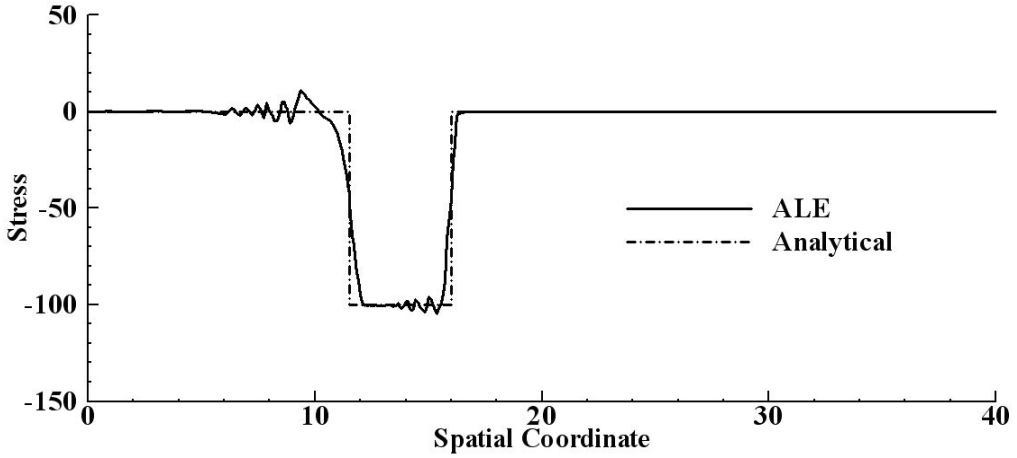

Fig. 2. Longitudinal stress distribution along the rod, elastic case

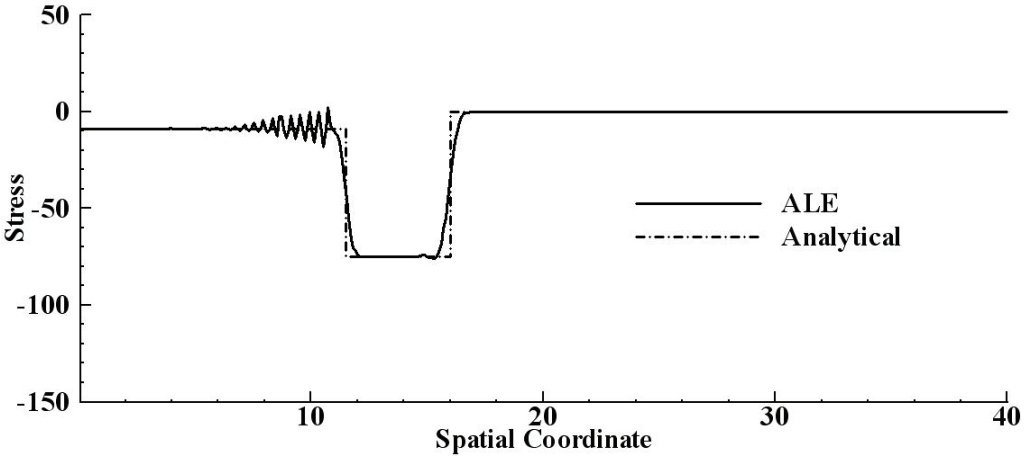

Fig. 3. Longitudinal stress distribution along the rod, elastic-plastic case

b) Necking in strip tension

In this example, the evolution of necking in a plane strain tensile specimen is investigated. This example demonstrates the capability of the presented ALE method in simulation of localized deformation. Figure 4 shows the geometry and initial mesh of the problem. A constant velocity v_0 in the horizontal direction is applied on the left side of the strip while the right-hand side is fixed. The material is assumed to be elastic plastic, linear hardening, with Young's modulus of 200 GPa, Poisson's ratio of 0.3, initial yield stress of 250 MPa and hardening parameter of 1.0 GPa. The Von Mises yield function with isotropic hardening is assumed and eight-node quadrilateral elements are used in this simulation. The dimensions of

the strip are $b_0 = 20$ mm and $r_0 = 2$ mm, and the strip width takes values of a_0 =10, 15, and 20 mm in the simulations.

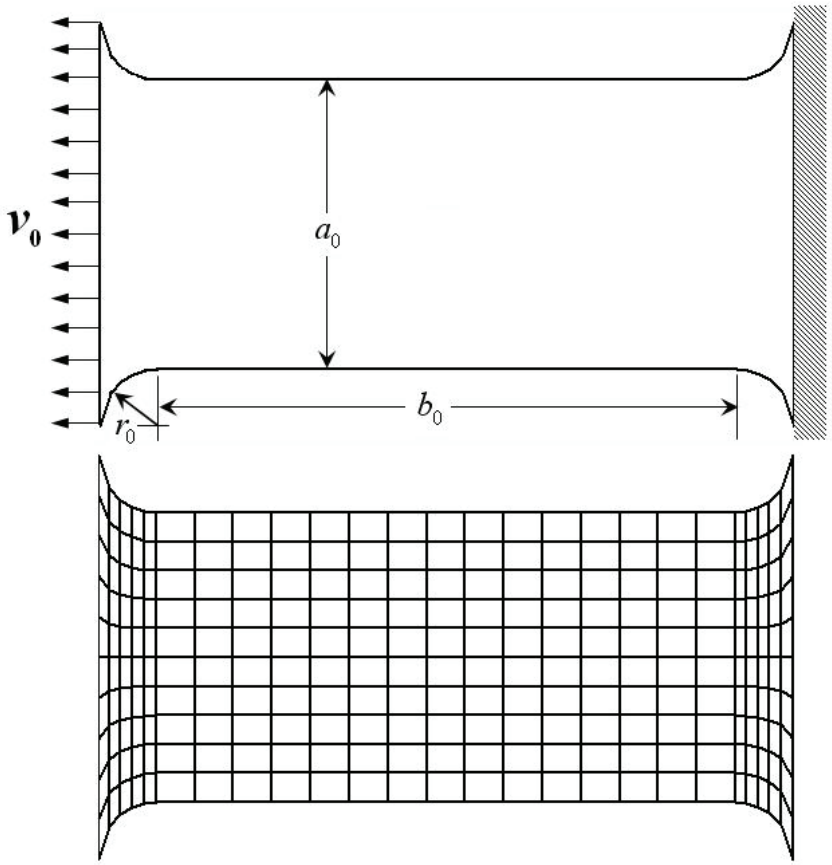

Fig. 4. Geometry and initial mesh for plane strain strip necking

The deformed shape and the finite element mesh after a total 4 mm of elongation of the strip are shown for various speeds in Fig. 5. It is observed that at lower speed, the deformation is spread in the balk of the strip, but as the speed increases, the deformation is localized close to the loaded side and severe necking is observed. Using the mesh motion capability in the ALE analysis, proper motion is assigned to the mesh to increase resolution at positions where local deformation is large.

The results of the above simulation may be compared to those presented by Rusinek, et al. [8]. They have solved the same problem using a 2D Lagrangian approach viscoplastic material model. In their paper, they have shown that in accordance with the experimental results of Wood [9], in quasi-static conditions the neck starts from the center of the specimen. At higher velocities ($v_0 \geq 19 \ \ m/s$), the inertial effects become more prominent and the necking site moves to the right (loaded side). The results presented here conform to this observation.

Figure 6 shows the deformed shape and the effective plastic strain contours after 4 mm of elongation at a velocity of 100 m/s for different widths of the specimen. It is interesting to note that in spite of the increase of the size of the specimen, the same number of elements is used without affecting the quality of the results. This demonstrates the capability of the ALE approach in obtaining reasonable results with a lower density mesh and in avoiding mesh distortion.

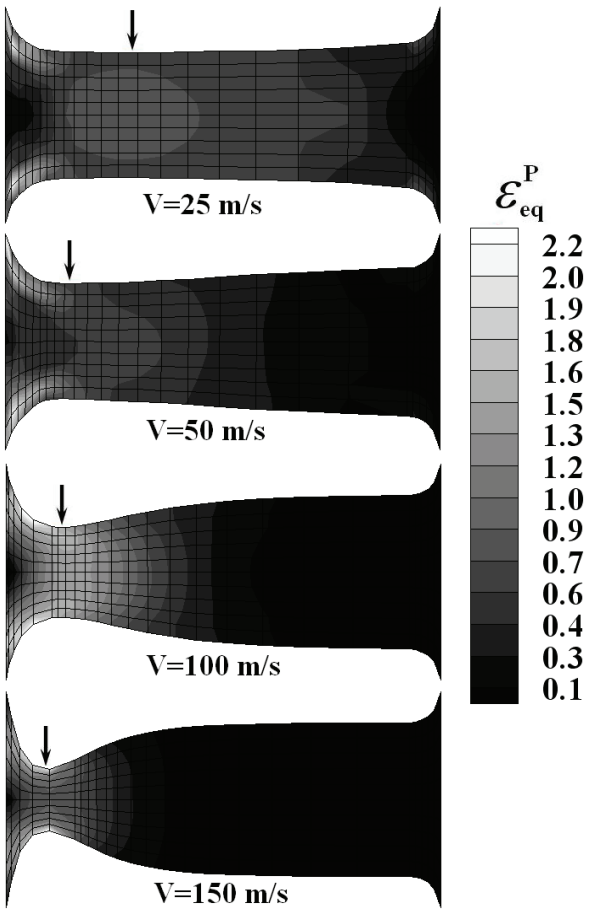

Fig. 5. Shape of necking and equivalent plastic strain at different velocities

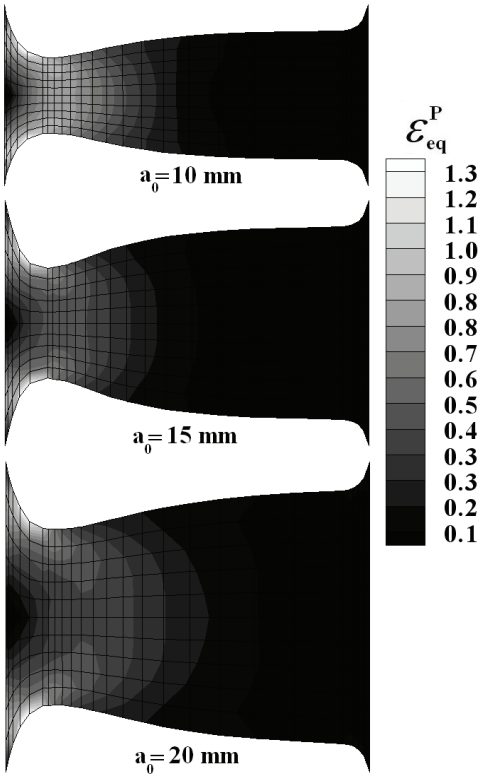

Fig. 6. Shape of necking and equivalent plastic strain at different geometry

c) Punch indentation problem

In this example, the punch indentation problem is simulated using the thermo-mechanical ALE formulation in both cold and hot forming states. The purpose of this example is to demonstrate the capability of ALE formulation in handling contact boundary conditions while preventing mesh distortion. A rigid tool indents into the workpiece at a prescribed velocity. Frictional contact exists between the tool and workpiece. Figure 7 shows the geometry and initial FE model of the problem. Because of the symmetry, only one quarter of the analysis domain is modelled. Eight-node quadrilateral elements are used. Thermal boundary conditions include air cooling at the free boundaries and adiabatic conditions at symmetric boundaries.

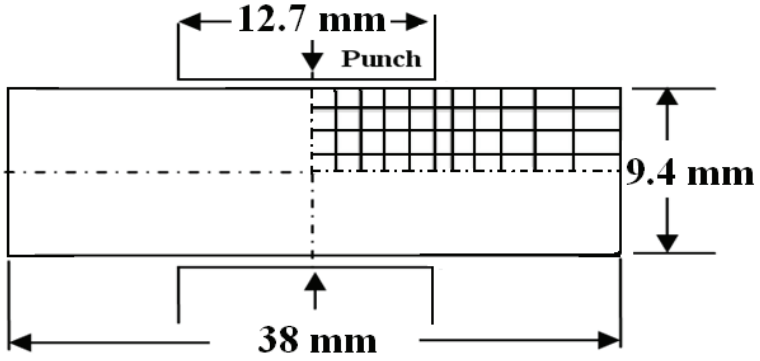

Fig. 7. Geometry and initial mesh for punch indentation

1. Cold punch indentation problem: Pietrzyk and Lenard [10] solved the cold punch indentation problem and presented numerical and experimental results. A similar problem is presented here using the ALE formulation. The dimensions and properties of the material are adopted from that reference for the purpose of comparison with experimental results. Rigid-plastic flow curve is defined as [10]:

$$\sigma_Y = 243.9\left(1+405\bar{\varepsilon}^{p}\right)^{0.097} \quad Mpa \tag{24}$$

The friction factor is assumed to be 0.12 on the contact surface. The specific heat and heat conduction coefficient are defined as functions of the temperature [10];

$$c_p = 0.62T + 836.8 \quad Jkg^{-1}K^{-1} \tag{25}$$

$$k = 0.033T + 236 \quad Wm^{-1}K^{-1} \tag{26}$$

The density also is expressed as

$$\rho = \rho_0 /(1 + 8.27\times10^{-12}T^{3} + 3.493\times10^{-9}T^{2} + 2.343\times10^{-5}T - 0.000457)^{3} \quad kgm^{-3} \tag{27}$$

where $\rho_0 = 4505 \quad kgm^{-3}$. The coefficient of convection is 20000 $Wm^{-2}k^{-1}$, the coefficient of thermal expansion is $2.4*10^{-5}$ k^{-1} and the Taylor-Quinney factor is 0.85. In order to model the frictional contact under the punch, a mesh motion scheme is designed that sets the degrees of freedom of the nodes directly under the punch to be Lagrangian in the vertical direction (to satisfy the boundary constraint) and Eulerian in the horizontal direction (to maintain the nodes under the punch). In addition, the designed mesh motion scheme, maintains a homogeneous mesh throughout the deformation. It is noted that in a

Lagrangian framework, the element near the corners of the die is severely distorted leading to deterioration of results as seen in reference [10], in spite of the remeshing steps used. Figure 8 shows the final distribution of effective plastic strain and temperature fields obtained from ALE solution. The figure shows that the contact condition between the punch and the workpiece is well represented.

In Fig. 9, variation of temperature at the center of the specimen is plotted for various reduction values and punch velocities. Comparing these values with the experimental result of reference [10] shows good agreement between them.

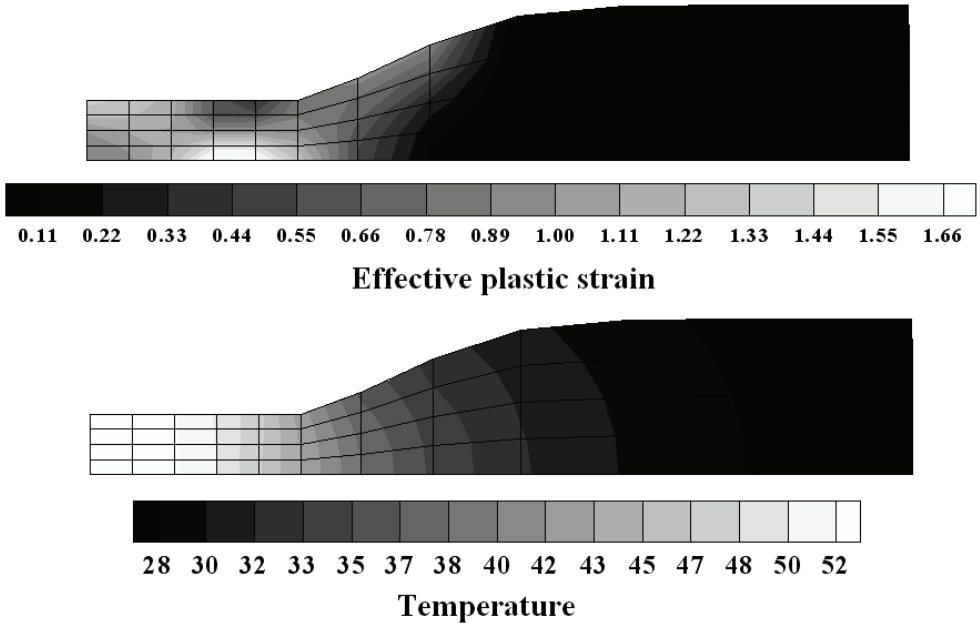

Fig. 8. Effective plastic strain and temperature distribution

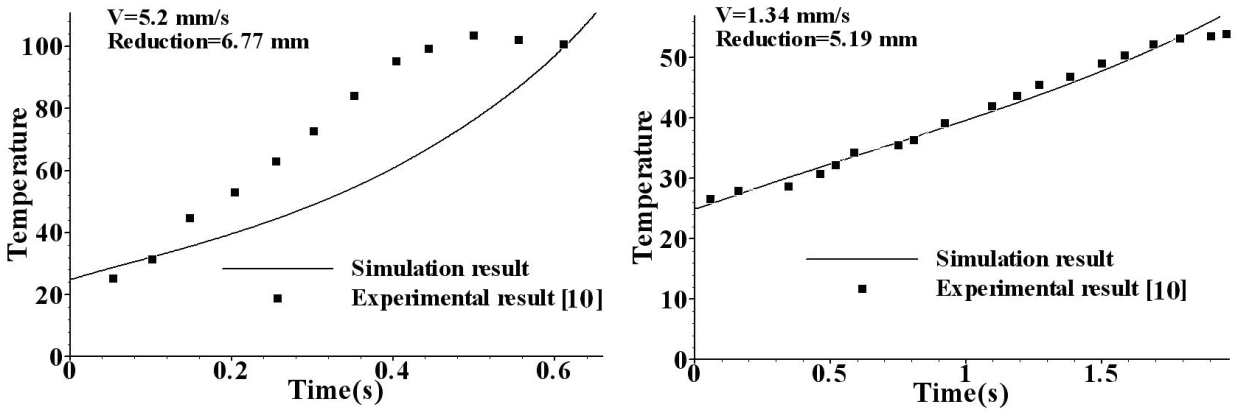

Fig. 9. Temperature rise during the deformation

2. Hot punch indentation problem: In this part of the example the hot punch indentation is simulated. The material properties are: density: 7830 kgm^{-3}, thermal conductivity: $53.49\,Wm^{-1}K^{-1}$, specific heat $460.52\,Jkg^{-1}K^{-1}$, friction factor 0.3, coefficient of heat convection in the die $2500\,Wm^{-2}K^{-1}$ and coefficient of heat convection in the air $25\,Wm^{-2}K^{-1}$. The initial temperature of the workpiece, die and atmosphere were set to be 1573 K, 773 K and 293 K, respectively. The rigid-viscoplastic flow curve is adopted from reference [11];

$$\sigma_Y = 82\left(\bar{\varepsilon}^p\right)^{-0.06}\left(\dot{\bar{\varepsilon}}^p\right)^{0.14} \; Mpa \tag{28}$$

The distribution of the effective plastic strain and temperature field after 50% reduction of thickness at a punch velocity of 10 mm/s is presented in Fig. 10.

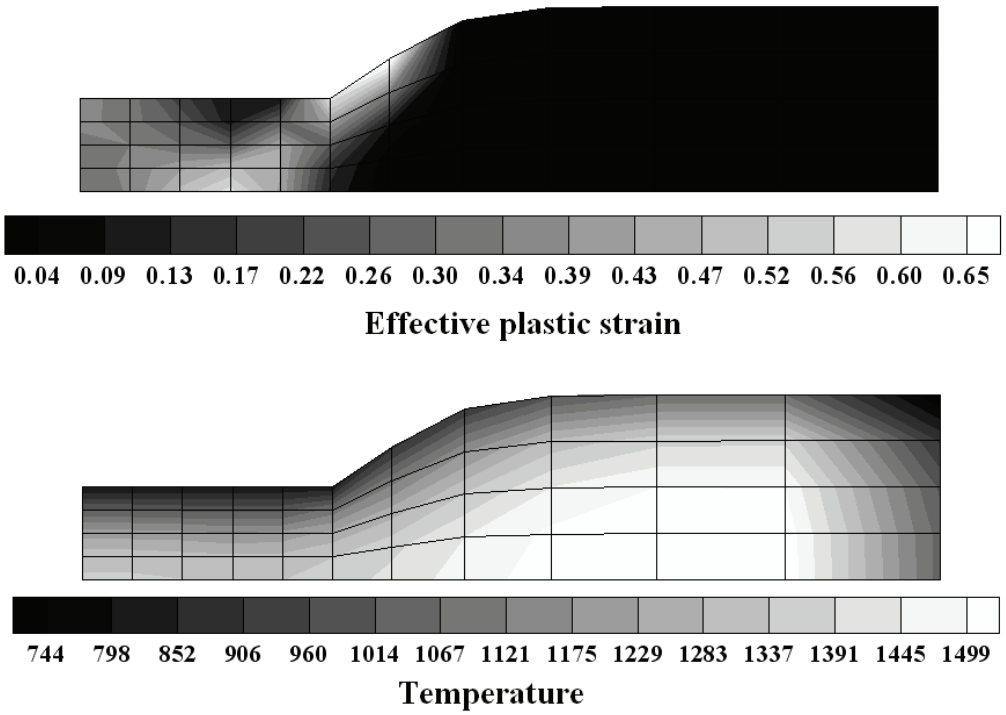

Fig. 10. Effective plastic strain and temperature distribution for punch indentation

By comparing this result with those in the cold forming example, it is observed that a large flow of thermal energy through the die has reduced the temperature of the material in contact with the die significantly; while the central parts of the specimen remain at higher temperatures.

d) Extrusion through a straight die

1. Cold extrusion: In this section, simulation of plane strain cold extrusion of aluminum metal strip is presented and the extrusion force obtained from simulation is compared with the experimental results of Farmer and Oxley [12]. The workpiece is 2.54mm thick ×10.16mm wide and its thickness is reduced to 1.27mm in the extrusion process. The friction on the die interface is minimized by effective lubrication. The material is 5052-H34 tempered aluminum and a linear hardening flow curve is assumed with a yield stress of 267.66 Mpa and strain hardening modulus of 85.85 Mpa. Other material properties are: Young's modulus 6.89×10^4 Mpa and Poisson's ratio 0.32[12]. Due to the symmetry of the geometry and boundary conditions, only half of the billet is modelled. The finite element mesh is shown in Fig. 11. In order to reduce the time to reach steady-state condition, the mesh is assumed to conform to the die at the start of analysis.

The contact boundary conditions between the die and the workpiece are applied by assigning all nodes in patch BCFG in Fig. 11 as Eulerian degrees of freedom (fixed in space). The motion of the nodes on the boundaries AB, CD, HG, AH, FE and ED is Lagrangian in Y direction and general ALE in X direction. The mesh motion scheme moves the nodes in x-direction in a way to maintain the regularity of the mesh. Displacement boundary conditions are applied to the nodes on the AH boundary. As the

material moves forward toward the extrusion die, the elements on the left of the die shrink and the elements to the right of the die expand to simulate the extrusion process. Figure 12 compares the extrusion forces obtained from ALE simulation in comparison with the experimental results of [12]. It is observed that the extrusion force from ALE is in close agreement with the experimental force.

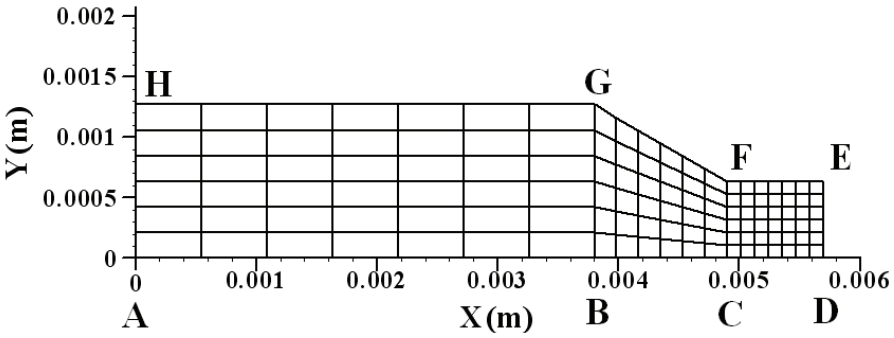

Fig. 11. Geometry and initial mesh for extrusion

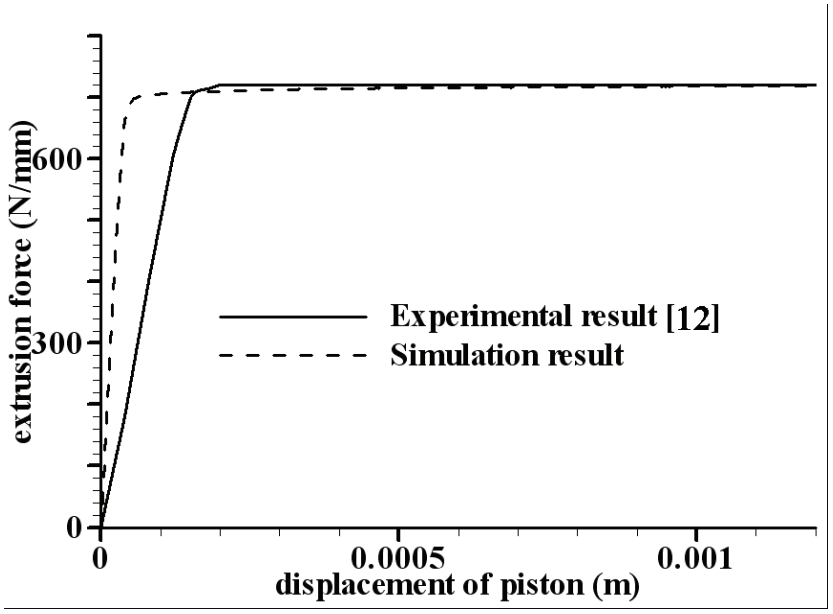

Fig. 12. comparison of extrusion force

2. Hot extrusion: In this section, the same extrusion problem is solved in hot deformation state for two reduction ratios of 50% and 25%. The initial temperature of work piece, die and atmosphere were set to be 470^0C, 400^0C and 25^0C, respectively. The friction coefficient was assumed to be 0.3. It is noted that the flow stress is important in the hot forming process [13], therefore the flow stress obtained from reference [14] for AL6061-T6 is:

$$\sigma_Y = 91\left(\dot{\bar{\varepsilon}}^p\right)^{0.09} \; Mpa \tag{29}$$

The distributions of effective plastic strain and temperature for 50% and 25% thickness reduction are shown in Figs. 13 and 14, respectively after 0.92 mm of ram movement.

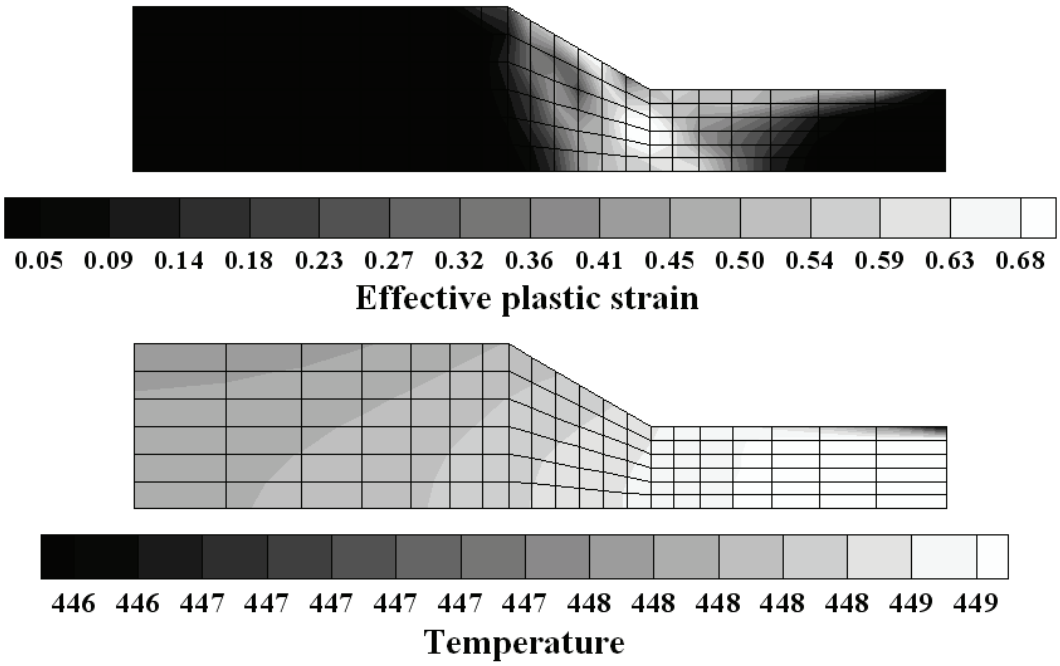

Fig. 13. Effective plastic strain and temperature distribution for 50% thickness reduction in extrusion

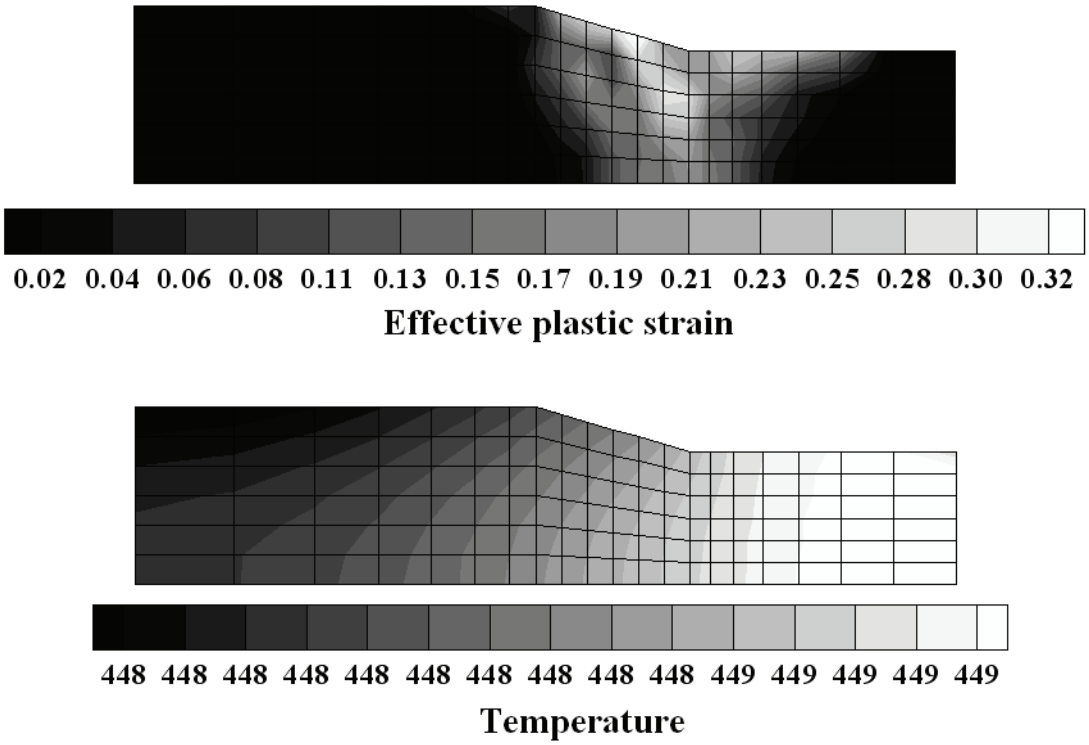

Fig. 14. Effective plastic strain and temperature distribution 25% thickness reduction in extrusion

5. CONCLUSION

This paper aimed at elucidating the power of the ALE finite element method to solve various static or dynamic large deformation problems of thermo-elasto-viscoplastic materials. Continuing on the first part of this paper series, the finite element discretization of fully coupled thermo-mechanical ALE formulation was presented and example simulation problems were presented. The examples demonstrate that the presented thermo-mechanical ALE formulation is capable of simulation of material deformation in cold or

hot states, with quasi-static or dynamic loading, and with a wide range of material models that include hardening, rate and/or thermal effects. Furthermore, the treatment of boundary conditions and maintaining mesh homogeneity throughout the analysis is conveniently carried out using a properly designed mesh motion scheme. Through the use of mesh motion, the ALE approach can enjoy a higher resolution mesh at the locations of highly localized deformation without having to increase the total number of elements.

REFERENCES

1. Bathe, K. J. (1996). *Finite element procedures*. Englewood Cliffs, NJ: Prentice-hall, Chapter 7, pp. 661-94.
2. Gadala, M. S., Movahhedy, M. R. & Wang, J. (2002). On the mesh motion for ALE modeling of metal forming processes. *Finite Elements in Analysis and Design*, Vol. 38, pp. 435-459.
3. Haber, R., Shepard, M. S., Abel, J. F., Gallagher, R. H. & Greenberg, D. P. (1981). A general two-dimentional, graphical finite element preprocessor utilizing discrete transfinite mapping. *Int. J. Numer. Methods Engrg*., Vol. 17, pp. 1015-1044.
4. Liu, W. K., Chang, H., Chen, J. S. & Belystchko, T. (1988). Arbitrary Lagrangian-Eulerian Petrov-Galerkin finite elements for nonlinear continua. *Comput. Methods Appl. Mech. Eng*., Vol. 68, pp. 259-310.
5. Bayoumi, H. N. & Gadala, M. S. (2004). A complete finite element treatment for the fully coupled implicit ALE formulation. *Computational Mechanics*, Vol. 33, pp. 435-452.
6. Liu, W. K., Belystchko, T. & Chang, H. (1986). An arbitrary Lagrangian-Eulerian finite elements method for patch-dependent materials. *Comput. Methods Appl. Mech. Eng*., Vol. 58, No. 2, pp. 227-245.
7. Huerta, A. & Casadei, F. (1994). New ALE applications in non-linear fast-transient solid dynamics. *Engineering Computations*, Vol. 11, pp. 317-345.
8. Rusinek, A., Zaera, R., Klepaczko, J. R. & Cheriguene, R. (2005). Analysis of inertia and scale effects on dynamic neck formation during tension of sheet steel. *Acta Materialia*, Vol. 53, pp. 5387-5400.
9. Wood, W.W. (1965). Experimental mechanics at velocity extremes-very high strain rates. *Exp Mech*, Vol. 5, pp. 361-371.
10. Pietrzyk, M. & Lanard, J.G. (1993). A study of the plane strain compression test. *Annals of the CIRP*, Vol. 42.
11. Guo, Y. M., Nakanishi, K. & Yokouchi, Y. (1999). A hot forging simulation by the volumetrically elastic and deviatorically rigid-plastic finite element method. *J. Materials Processing Technology*, Vol. 89-90, pp. 111-116.
12. Framer, L. E. & Oxley, P. L. B. (1971). A slip field for plane strain extrusion of a atrain-hardening material. *J. Mech. Phys. solid*, Vol. 19, pp 369-388.
13. Moslemi Naeini, H., Maerefat, M. & Soltanpour, M., "Finite element simulation of hot forming process by using flow stress prediction model. *Iranian Journal of Science & Technology, Transaction B, Engineering*, Vol. 29, No.B2, pp 231-240.
14. Lee, G. A., Kwak, D. Y., Kim, S. Y. & Im, Y. T. (2002). Analysis and design of flat-die hot extrusion process: 1. Three dimensional finite element analysis. *I. J. Mechanical Sciences*, Vol. 44, pp 915-934.

APPENDIX

If we assume the number of element nodal points are N, and h_k is the element shape function corresponding to nodal point k, matrices ${}_t\mathbf{B}^L$, ${}_t\mathbf{B}^{A1}$, ${}_t\mathbf{B}^{A2}$, ${}_t\mathbf{B}^{A3}$, ${}^t\mathbf{S}^{A1}$, ${}^t\mathbf{S}^{A2}$, ${}^t\mathbf{S}^{A3}$ and $\mathbf{H}$ are given by

$$ {}_t\mathbf{B}^L = \begin{bmatrix} \frac{\partial h_k}{\partial {}^t x} & 0 \\ \cdots \quad 0 & \frac{\partial h_k}{\partial {}^t y} \quad \cdots \\ \frac{\partial h_k}{\partial {}^t y} & \frac{\partial h_k}{\partial {}^t x} \end{bmatrix}_{3\times 2N} \tag{A.1} $$

$$ {}_t\mathbf{B}^{A1} = \begin{bmatrix} \frac{\partial h_k}{\partial {}^t x} & 0 \\ \frac{\partial h_k}{\partial {}^t y} & 0 \\ \cdots & \cdots \\ 0 & \frac{\partial h_k}{\partial {}^t x} \\ 0 & \frac{\partial h_k}{\partial {}^t y} \end{bmatrix}_{4\times 2N} \tag{A.2} $$

$$ {}_t\mathbf{B}^{A2} = \begin{bmatrix} \frac{\partial h_k}{\partial {}^t x} & \\ & \frac{\partial h_k}{\partial {}^t x} \\ \cdots \frac{\partial h_k}{\partial {}^t y} & \cdots \\ & \frac{\partial h_k}{\partial {}^t y} \end{bmatrix}_{4\times 2N} \tag{A.3} $$

$$ {}_t\mathbf{B}^{A3} = \begin{bmatrix} \frac{\partial^2 h_k}{\partial {}^t x^2} & 0 \\ \frac{\partial^2 h_k}{\partial {}^t y^2} & 0 \\ \frac{\partial^2 h_k}{\partial {}^t x\, \partial {}^t y} & 0 \\ 0 & \frac{\partial^2 h_k}{\partial {}^t x^2} \\ 0 & \frac{\partial^2 h_k}{\partial {}^t y^2} \\ 0 & \frac{\partial^2 h_k}{\partial {}^t x\, \partial {}^t y} \end{bmatrix}_{6\times 2N} \tag{A.4} $$

$$ {}_t\mathbf{S}^{A1} = \begin{bmatrix} {}^t\sigma_{xx} & {}^t\sigma_{xy} & 0 & 0 \\ {}^t\sigma_{yx} & {}^t\sigma_{yy} & 0 & 0 \\ 0 & 0 & {}^t\sigma_{xx} & {}^t\sigma_{xy} \\ 0 & 0 & {}^t\sigma_{yx} & {}^t\sigma_{yy} \end{bmatrix}_{4\times 4} \tag{A.5} $$

$$ {}_t\mathbf{S}^{A2} = \begin{bmatrix} {}^t\sigma_{xx} & 0 & {}^t\sigma_{xy} & {}^t\sigma_{xy} & 0 & {}^t\sigma_{yy} \\ 0 & {}^t\sigma_{xy} & {}^t\sigma_{xx} & 0 & {}^t\sigma_{yy} & {}^t\sigma_{xy} \end{bmatrix}_{2\times 6} \tag{A.6} $$

$$ {}_t\mathbf{S}^{A3} = \begin{bmatrix} {}^t\sigma_{xx} & 0 & 0 & {}^t\sigma_{xx} \\ {}^t\sigma_{xy} & 0 & 0 & {}^t\sigma_{xy} \\ {}^t\sigma_{yx} & 0 & 0 & {}^t\sigma_{yx} \\ {}^t\sigma_{yy} & 0 & 0 & {}^t\sigma_{yy} \end{bmatrix}_{4\times 4} \tag{A.7} $$

$$ \mathbf{H} = \begin{bmatrix} h_k & 0 \\ \cdots & \cdots \\ 0 & h_k \end{bmatrix}_{2\times 2N} \tag{A.8} $$

Matrix ${}^t\mathbf{N}^1$ is given by

$$ {}^{t}\mathbf{N}^{1}=\begin{bmatrix} & \vdots & \\ \cdots & {}^{t}N^{1}{}_{2i-1,2j-1} \quad {}^{t}N^{1}{}_{2i-1,2j} & \cdots \\ & {}^{t}N^{1}{}_{2i,2j-1} \quad {}^{t}N^{1}{}_{2i,2j} & \\ & \vdots & \end{bmatrix} \tag{A.9} $$

In which

$$ {}^{t}N^{1}{}_{2i-1,2j-1}={}^{t}N^{1}{}_{2i,2j}=\int_{{}^{t}V}{}^{t}\rho[h_i\frac{\partial h_j}{\partial {}^{t}x}\sum_{k=1}^{N}h_k({}^{t}\overline{v}_{xk}-{}^{t}\overline{v}^{g}_{xk})+h_i\frac{\partial h_j}{\partial {}^{t}y}\sum_{k=1}^{N}h_k({}^{t}\overline{v}_{yk}-{}^{t}\overline{v}^{g}_{yk})]{}^{t}dV \tag{A.10} $$

$$ {}^{t}N^{1}{}_{2i-1,2j}={}^{t}N^{1}{}_{2i,2j-1}=0 \tag{A.11} $$

Matrix ${}^{t}\mathbf{N}^{2}$ is given by

$$ {}^{t}\mathbf{N}^{2}=\begin{bmatrix} & \vdots & \\ \cdots & {}^{t}N^{2}{}_{2i-1,2j-1} \quad {}^{t}N^{2}{}_{2i-1,2j} & \cdots \\ & {}^{t}N^{2}{}_{2i,2j-1} \quad {}^{t}N^{2}{}_{2i,2j} & \\ & \vdots & \end{bmatrix} \tag{A.12} $$

In which

$$ \begin{aligned} &{}^{t}N^{2}{}_{2i-1,2j-1}={}^{t}N^{2}{}_{2i,2j}=\int_{{}^{t}V}{}^{t}\rho\{[h_i\frac{\partial h_j}{\partial {}^{t}x}\sum_{k=1}^{N}\frac{\partial h_k}{\partial {}^{t}x}({}^{t}\overline{v}_{xk}-{}^{t}\overline{v}^{g}_{xk})+h_i\frac{\partial h_j}{\partial {}^{t}y}\sum_{k=1}^{N}\frac{\partial h_k}{\partial {}^{t}x}({}^{t}\overline{v}_{yk}-{}^{t}\overline{v}^{g}_{yk})]\\ &\sum_{k=1}^{N}h_k({}^{t}\overline{v}_{xk}-{}^{t}\overline{v}^{g}_{xk})+[h_i\frac{\partial h_j}{\partial {}^{t}x}\sum_{k=1}^{N}\frac{\partial h_k}{\partial {}^{t}y}({}^{t}\overline{v}_{xk}-{}^{t}\overline{v}^{g}_{xk})+h_i\frac{\partial h_j}{\partial {}^{t}y}\sum_{k=1}^{N}\frac{\partial h_k}{\partial {}^{t}y}({}^{t}\overline{v}_{yk}-{}^{t}\overline{v}^{g}_{yk})]\\ &\sum_{k=1}^{N}h_k({}^{t}\overline{v}_{yk}-{}^{t}\overline{v}^{g}_{yk})+(\frac{\partial h_i}{\partial {}^{t}x}\frac{\partial h_j}{\partial {}^{t}y}+\frac{\partial h_i}{\partial {}^{t}y}\frac{\partial h_j}{\partial {}^{t}x}+2h_i\frac{\partial^{2}h_j}{\partial {}^{t}x\partial {}^{t}y})\\ &\sum_{k=1}^{N}h_k({}^{t}\overline{v}_{xk}-{}^{t}\overline{v}^{g}_{xk})\sum_{k=1}^{N}h_k({}^{t}\overline{v}_{yk}-{}^{t}\overline{v}^{g}_{yk})+(\frac{\partial h_i}{\partial {}^{t}x}\frac{\partial h_j}{\partial {}^{t}x}+h_i\frac{\partial^{2}h_j}{\partial {}^{t}x^{2}})(\sum_{k=1}^{N}h_k({}^{t}\overline{v}_{xk}-{}^{t}\overline{v}^{g}_{xk}))^{2}+\\ &(\frac{\partial h_i}{\partial {}^{t}y}\frac{\partial h_j}{\partial {}^{t}y}+h_i\frac{\partial^{2}h_j}{\partial {}^{t}y^{2}})(\sum_{k=1}^{N}h_k({}^{t}\overline{v}_{yk}-{}^{t}\overline{v}^{g}_{yk}))^{2}\}\Delta t\,{}^{t}dV \end{aligned} \tag{A.13} $$

$$ {}^{t}N^{2}{}_{2i-1,2j}={}^{t}N^{2}{}_{2i,2j-1}=0 \tag{A.14} $$

Matrix ${}^{t}\mathbf{N}^{3}$ is given by

$$ {}^{t}\mathbf{N}^{3}=\begin{bmatrix} & \vdots & \\ \cdots & {}^{t}N^{3}{}_{2i-1,2j-1} \quad {}^{t}N^{3}{}_{2i-1,2j} & \cdots \\ & {}^{t}N^{3}{}_{2i,2j-1} \quad {}^{t}N^{3}{}_{2i,2j} & \\ & \vdots & \end{bmatrix} \tag{A.15} $$

In which

$$ \begin{aligned} &{}^{t}N^{3}{}_{2i-1,2j-1}={}^{t}N^{3}{}_{2i,2j}=\int_{{}^{t}V}{}^{t}\rho\{[h_i\frac{\partial h_j}{\partial {}^{t}x}\sum_{k=1}^{N}\frac{\partial h_k}{\partial x}{}^{t}\overline{v}^{g}_{xk}+h_i\frac{\partial h_j}{\partial {}^{t}y}\sum_{k=1}^{N}\frac{\partial h_k}{\partial x}{}^{t}\overline{v}^{g}_{yk}]\\ &\sum_{k=1}^{N}h_k({}^{t}\overline{v}_{xk}-{}^{t}\overline{v}^{g}_{xk})+[h_i\frac{\partial h_j}{\partial {}^{t}x}\sum_{k=1}^{N}\frac{\partial h_k}{\partial y}{}^{t}\overline{v}^{g}_{xk}+h_i\frac{\partial h_j}{\partial {}^{t}y}\sum_{k=1}^{N}\frac{\partial h_k}{\partial y}{}^{t}\overline{v}^{g}_{yk}]\sum_{k=1}^{N}h_k({}^{t}\overline{v}_{yk}-{}^{t}\overline{v}^{g}_{yk})\}\Delta t\,{}^{t}dV \end{aligned} \tag{A.16} $$

$$ {}^{t}N^{3}{}_{2i-1,2j}={}^{t}N^{3}{}_{2i,2j-1}=0 \tag{A.17} $$

Matrix ${}^{t}\mathbf{N}^{4}$ is given by

$$ {}^{t}\mathbf{N}^{4} = \begin{bmatrix} & \vdots & \\ \cdots & {}^{t}N^{4}_{2i-1,2j-1} \quad {}^{t}N^{4}_{2i-1,2j} & \cdots \\ & {}^{t}N^{4}_{2i,2j-1} \quad {}^{t}N^{4}_{2i,2j} & \\ & \vdots & \end{bmatrix} \tag{A.18} $$

In which

$$ {}^{t}N^{4}_{2i-1,2j-1} = {}^{t}N^{4}_{2i,2j} = \int_{{}^{t}V} {}^{t}\rho[h_i \frac{\partial h_j}{\partial {}^{t}x} \sum_{k=1}^{N} h_k ({}^{t}\overline{a}_{xk} - {}^{t}\overline{a}^{g}_{xk}) + h_i \frac{\partial h_j}{\partial {}^{t}y} \sum_{k=1}^{N} h_k ({}^{t}\overline{a}_{yk} - {}^{t}\overline{a}^{g}_{yk})]\Delta t \, {}^{t}dV \tag{A.19} $$

$$ {}^{t}N^{4}_{2i-1,2j} = {}^{t}N^{4}_{2i,2j-1} = 0 \tag{A.20} $$

Matrix ${}^{t}\mathbf{M}^{A}$ is given by

$$ {}^{t}\mathbf{M}^{A} = \begin{bmatrix} & \vdots & \\ \cdots & {}^{t}M^{A}_{2i-1,2j-1} \quad {}^{t}M^{A}_{2i-1,2j} & \cdots \\ & {}^{t}M^{A}_{2i,2j-1} \quad {}^{t}M^{A}_{2i,2j} & \\ & \vdots & \end{bmatrix} \tag{A.21} $$

In which

$$ \begin{aligned} {}^{t}M^{A}_{2i-1,2j-1} = {}^{t}M^{A}_{2i,2j} = \int_{{}^{t}V} {}^{t}\rho[(h_i \frac{\partial h_j}{\partial {}^{t}x} + h_j \frac{\partial h_i}{\partial {}^{t}x}) \sum_{k=1}^{N} h_k ({}^{t}\overline{v}_{xk} - {}^{t}\overline{v}^{g}_{xk}) + \\ (h_i \frac{\partial h_j}{\partial {}^{t}y} + h_j \frac{\partial h_i}{\partial {}^{t}y}) \sum_{k=1}^{N} h_k ({}^{t}\overline{v}_{yk} - {}^{t}\overline{v}^{g}_{yk})]\Delta t \, {}^{t}dV \end{aligned} \tag{A.22} $$

$$ {}^{t}M^{A}_{2i-1,2j} = {}^{t}M^{A}_{2i,2j-1} = 0 \tag{A.23} $$

$$ {}_{t}\mathbf{B} = \begin{bmatrix} \frac{\partial h_k}{\partial {}^{t}x} \\ \cdots \\ \frac{\partial h_k}{\partial {}^{t}y} \end{bmatrix}_{2\times N} \cdots \tag{A.24} $$

$$ {}^{t+\Delta t}\mathbf{C}_{\mathrm{A}}^{(\mathrm{i}-1)} = \begin{bmatrix} & \vdots & \\ \cdots & {}^{t+\Delta t}\mathrm{C}_{\mathrm{A}}^{(\mathrm{i}-1)}{}_{i,j} & \cdots \\ & \vdots & \end{bmatrix} \tag{A.25} $$

in which

$$ {}^{t+\Delta t}\mathrm{C}_{\mathrm{A}}^{(\mathrm{i}-1)}{}_{i,j} = \int_{{}^{t+\Delta t}V} {}^{t+\Delta t}(\rho c_v)[h_i \frac{\partial h_j}{\partial {}^{t}x} \sum_{k=1}^{N} h_k ({}^{t}\overline{v}_{xk} - {}^{t}\overline{v}^{g}_{xk}) + h_i \frac{\partial h_j}{\partial {}^{t}y} \sum_{k=1}^{N} h_k ({}^{t}\overline{v}_{yk} - {}^{t}\overline{v}^{g}_{yk})]^{t+\Delta t}dV \tag{A.26} $$

$$ \mathbf{H} = \begin{bmatrix} \cdots h_k \cdots \end{bmatrix}_{1\times N} \tag{A.27} $$

$$ {}^{t+\Delta t}\mathbf{Q}_{\mathrm{A1}}^{(\mathrm{i}-1)} = \begin{bmatrix} \vdots \\ {}^{t+\Delta t}\mathrm{Q}_{\mathrm{A1\,ij}}^{(\mathrm{i}-1)} \\ \vdots \end{bmatrix}_{N\times 1} \tag{A.28} $$

in which

$$
\begin{aligned}
{}^{t+\Delta t}\mathrm{Q}^{(\mathrm{i\text{-}1})}_{\mathrm{A1\,ij}} = \int_{{}^{t+\Delta t}V} {}^{t+\Delta t}(\rho c_v)\Bigg\{\Bigg[h_i \frac{\partial h_j}{\partial {}^t x}\sum_{k=1}^{N} h_k ({}^t\bar{v}_{xk} - {}^t\bar{v}^g_{xk}) + h_i \frac{\partial h_j}{\partial {}^t y}\sum_{k=1}^{N} h_k ({}^t\bar{v}_{yk} - {}^t\bar{v}^g_{yk})\Bigg] - \\
\Bigg[h_i \frac{\partial h_j}{\partial {}^t x}\sum_{k=1}^{N}\frac{\partial h_k}{\partial {}^t x}{}^t\bar{v}^g_{xk} + h_i \frac{\partial h_j}{\partial {}^t y}\sum_{k=1}^{N}\frac{\partial h_k}{\partial {}^t x}{}^t\bar{v}^g_{yk}\Bigg]\sum_{k=1}^{N} h_k ({}^t\bar{v}_{xk} - {}^t\bar{v}^g_{xk}) - \\
\Bigg[h_i \frac{\partial h_j}{\partial {}^t x}\sum_{k=1}^{N}\frac{\partial h_k}{\partial {}^t y}{}^t\bar{v}^g_{xk} + h_i \frac{\partial h_j}{\partial {}^t y}\sum_{k=1}^{N}\frac{\partial h_k}{\partial {}^t y}{}^t\bar{v}^g_{yk}\Bigg]\sum_{k=1}^{N} h_k ({}^t\bar{v}_{yk} - {}^t\bar{v}^g_{yk})\Bigg\}\Delta t\, {}^{t+\Delta t}T^{\,(i-1)}\, {}^{t+\Delta t}dV
\end{aligned}
\tag{A.29}
$$

$$
{}^{t+\Delta t}\mathbf{Q}^{(\mathrm{i\text{-}1})}_{\mathrm{A2}} = \begin{bmatrix} \vdots \\ {}^{t+\Delta t}\mathrm{Q}^{(\mathrm{i\text{-}1})}_{\mathrm{A2\,ij}} \\ \vdots \end{bmatrix}_{N\times 1}
\tag{A.30}
$$

in which

$$
\begin{aligned}
{}^{t+\Delta t}\mathrm{Q}^{(\mathrm{i\text{-}1})}_{\mathrm{A2\,ij}} = \int_{{}^{t+\Delta t}V} {}^{t+\Delta t}k^{\,(i-1)}\Bigg\{\frac{\partial h_i}{\partial {}^t x}\Bigg[\frac{\partial h_j}{\partial {}^t x}\sum_{k=1}^{N}\frac{\partial h_k}{\partial {}^t x}{}^t\bar{v}^g_{xk} + \frac{\partial h_j}{\partial {}^t y}\sum_{k=1}^{N}\frac{\partial h_k}{\partial {}^t x}{}^t\bar{v}^g_{yk}\Bigg] + \\
\frac{\partial h_i}{\partial {}^t y}\Bigg[\frac{\partial h_j}{\partial {}^t x}\sum_{k=1}^{N}\frac{\partial h_k}{\partial {}^t y}{}^t\bar{v}^g_{xk} + \frac{\partial h_j}{\partial {}^t y}\sum_{k=1}^{N}\frac{\partial h_k}{\partial {}^t y}{}^t\bar{v}^g_{yk}\Bigg] + \Bigg[\frac{\partial h_i}{\partial {}^t x}\sum_{k=1}^{N}\frac{\partial h_k}{\partial {}^t x}{}^t\bar{v}^g_{xk} + \frac{\partial h_i}{\partial {}^t y}\sum_{k=1}^{N}\frac{\partial h_k}{\partial {}^t x}{}^t\bar{v}^g_{yk}\Bigg]\frac{\partial h_j}{\partial {}^t x} + \\
\Bigg[\frac{\partial h_i}{\partial {}^t x}\sum_{k=1}^{N}\frac{\partial h_k}{\partial {}^t y}{}^t\bar{v}^g_{xk} + \frac{\partial h_i}{\partial {}^t y}\sum_{k=1}^{N}\frac{\partial h_k}{\partial {}^t y}{}^t\bar{v}^g_{yk}\Bigg]\frac{\partial h_j}{\partial {}^t y}\Bigg\}\Delta t\, {}^{t+\Delta t}T^{\,(i-1)}\, {}^{t+\Delta t}dV
\end{aligned}
\tag{A.31}
$$